agronomy

MDPI

Article

Temperature Dependences of IR Spectral Bands of Humic Substances of Silicate-Based Soils

Mikhail A. Proskurnin [1,*], Dmitry S. Volkov [1,2] and Olga B. Rogova [1,2]

[1] Chemistry Department, M.V. Lomonosov Moscow State University, Leninskie Gory, 1-3, GSP-1, 119991 Moscow, Russia; dmsvolkov@gmail.com (D.S.V.); obrogova@gmail.com (O.B.R.)
[2] Department of Chemistry and Physical Chemistry of Soils, V.V. Dokuchaev Soil Science Institute, Pyzhevsky per., 7/2, 119017 Moscow, Russia
* Correspondence: proskurnin@gmail.com or michael@analyt.chem.msu.ru

Abstract: Temperature-dependent IR spectroscopy capable of revealing specific changes in the band intensities, positions, and shape was used to increase the information on humic substances (HS) from soils. Temperature dependences of IR spectra of HS isolated from silicate-based soils differing in the contents and nature of organic matter, chernozem and soddy podzolic soil, were investigated by attenuated total internal reflection FTIR in the mid-IR region (4000–400 cm^{-1}) in the air within the moderate temperature range of 25–215 °C (298–488 K) with a step of 2.5 °C. The dependences of shifts in frequency (wavenumber) corresponding to band maxima and integrated band intensities were built for all major bands. Observed reversible frequency shifts upon heating and cooling can be interpreted as forming structures in the dry state. The behavior of integrated intensities of bands assigned to C–H and C–C vibrations, characteristic vibrations of polyaromatic compounds, carboxylic acids, and carboxylates were shown, and similar behavior for the same group (symmetric and antisymmetric stretches) were revealed. Differences in the temperature trends in chernozem and soddy podzolic soils due to different structures (aliphatic and aromatic) and functional groups (carboxylic and carboxylate) are shown. The different behavior of the bands corresponding to carboxylic groups and skeletal vibrations differentiates soil types with different organic matter. The temperature trends of band maximum and intensity shifts are less prone to measurement conditions and may serve as qualitative parameters characterizing the composition of soil humic substances.

Keywords: FTIR spectroscopy; infrared spectroscopy; attenuated total internal reflection; temperature-dependent infrared spectra; molecular structure; soil organic matter; humic substances; chernozem; soddy podzolic soil

check for updates

Citation: Proskurnin, M.A.; Volkov, D.S.; Rogova, O.B. Temperature Dependences of IR Spectral Bands of Humic Substances of Silicate-Based Soils. *Agronomy* **2023**, *13*, 1740. https://doi.org/10.3390/agronomy13071740

Academic Editor: Maria Roulia

Received: 9 June 2023
Revised: 23 June 2023
Accepted: 26 June 2023
Published: 28 June 2023

Copyright: © 2023 by the authors. Licensee MDPI, Basel, Switzerland. This article is an open access article distributed under the terms and conditions of the Creative Commons Attribution (CC BY) license (https://creativecommons.org/licenses/by/4.0/).

1. Introduction

Humic substances (HS) are predominant in soil organic matter (SOM), aquatic, and other environmental entities as well as in human-made or altered objects such as sewage, landfills, and urban environments [1–4]. In the pedosphere, HS are involved in chemical and biochemical processes of soil formation, degradation, and recultivation [5,6]. From the practical—agricultural and agronomic—viewpoints, HS are used as fertilizers, plant growth regulators, mediators, and detoxifiers in polluted ecosystems [6–12]. HS are also relevant in coal and biomass treatment [13–15]. Furthermore, HS separated from sediments, peat, or lignites are applied as antibacterial, antiviral, immunomodulating, and other medicines or antioxidants [8,9,16].

Thus, the chemical analysis of HS is required in various areas. Of prime importance is soil HS analysis due to HS involvement in natural processes such as soil formation [17–19] and in understanding soil diversity and the changes upon agricultural use as well as in targeted soil remediation [20–22]. All these underlying processes require both a large volume of information on HS systems and significant reliability and precision. This, in turn, implies the development of corresponding analysis and characterization methods.

IR spectroscopy is a prime analysis method for soils, SOM, and HS organic matter (HSOM) [23–27], and its role constantly increases due to new technological levels in detection sensitivity, precision, and overall instrumental and methodological capabilities [28,29]. The information on HS and HSOM from conventional IR spectroscopy is still limited and constrained by qualitative comparison of the functional-group composition [30,31]. However, the potential of IR spectroscopy for soils is far from being fully explored. Changes in the vibrational spectra of solid samples upon heating or cooling provide the information on polymorphic transformations, structural phase transitions, intramolecular interactions, and second-order phase transitions [32,33]. Furthermore, temperature-dependent IR spectra reveal selective changes in the band intensities, positions, shape, and width [32] that can be used both for soil identification and classification and quantification of HS and SOM.

For HS, temperature dependences of IR spectra are still used relatively seldom, especially in the moderate temperature ranges where there are no significant or irreversible molecular structure changes. There are studies on IR spectra of soil HS upon heating at temperatures over 325 °C [34] or upon simulating fire conditions [35]. Moisture effects on IR spectra were studied by a conventional KBr-pellet transmission technique [36]. Furthermore, in the range of 150–400 °C, decarboxylation was found to be the primary process responsible for HS dehydration, and anhydride in HS was identified from IR spectra at 200–400 °C [37]. Along with other methods, IR spectra at 20–800 °C were used to elucidate the thermal stability of soil HS [38]. It is noteworthy that only the major features of IR spectra—OH-stretching continuum at 3450 cm^{-1}, main C–H stretching bands at 2920 and 2850 cm^{-1}, and vibrations of carboxylic groups at 1720 cm^{-1}—were studied as macroscopic effects in the spectra. More recently, we used temperature dependences in the moderate temperature range for differentiating humic substances from brown coal [39]. IR spectroscopy distinguishes bands of crystalline and amorphous SiO_2 species and the HSOM part of these samples due to different temperature shifts of band maxima [39]. However, this study involved HS sample separated from brown coal and with incomplete technological separation from silicate matrices, which can be improved by more selective preparative techniques [40]. This is especially important for soil HS as it shows much broader diversity of SOM and interaction of organic and inorganic components.

Therefore, this work aims to implement the capabilities of temperature-dependent IR spectroscopy to increase the information on humic substances of soils differing in the contents and nature of SOM—soddy podzolic and chernozem soils. The temperature dependences of IR spectra of HS were studied in the temperature range of 25 to 215 °C, i.e., mild conditions with no destructive changes in HS.

2. Materials and Methods

2.1. Soil Humic Substance Samples

HS from certified reference samples of soddy podzolic soil (Russian State certified reference material, GSO 10863-2016) under forest vegetation (boreonemoral forest) and typical chernozem of the Kursk region (Russian State certified reference material, GSO 10862-2016) under grain row crop rotation. Soil samples were taken from the territories of the experimental bases of Lomonosov Moscow State University, Chashnikovo (Moscow Region) and V.V. Dokuchaev Soil Institute, the former Petrinsky experimental site in the Kursk Region. The soils were comprehensively studied previously, and the results are presented in a number of papers, monographs, and guidebooks; major elements in SOM are summed up in Table 1 [40–42].

Table 1. Standardized parameters of major elements in HS from soil reference materials (p = 0.95) [40–42].

Sample	Parameter	Min–Max	±Δ, %
Soddy podzolic soil, GSO 10863-2016,	C, % w/w	40.0–56.0	1.1
	H, % w/w	3.50–6.50	0.7
	N, % w/w	3.50–6.70	0.7
	H/C, mol:mol	1.05−1.39	3
	C/N, mol:mol	9.9−13.2	3
Chernozem, GSO 10862-2016	C, % w/w	45.0–59.0	1.1
	H, % w/w	2.50–5.50	0.7
	N, % w/w	2.70–5.70	0.7
	H/C, mol:mol	0.66−1.12	3
	C/N, mol:mol	12.0−19.7	3

The ash content is not more than 5%.

Soddy podzolic soils are developed in the boreal zone (the subzone of the middle taiga) in a humid climate; the soil-forming rock covers loam on moraine deposits represented by heavy red-brown loam of very dense composition with negligible water permeability. The SOM content is less than 1%, pH (KCl) is 4.3–5.3 [43].

The site of the long-term field experiment on a typical chernozem is located in the forest-steppe zone of the Central Russian Upland, in a moderately cold climate with a moisture coefficient of less than 1. The soils are developed on carbonate loess-like loams with high porosity. The SOM content is 3.2–3.5% w/w, the reaction of the medium is slightly acidic to neutral [40,44,45].

The content of macro- and microelements for additional information was determined by inductively coupled plasma atomic emission spectroscopy (ICP-AES) after acid decomposition of the samples [46]; see Section 2.3 for other details.

2.2. Humic Substance Samples

HS preparations were isolated from contrasting soils in terms of the conditions of formation and existence. HS were separated according to the previously developed procedure with the maximum removal of the inorganic matrix [40]. An average soil sample of 2 kg was used, the suspension was decalcified by 1 M HCl to a pH of 1.0–2.0, then 0.1 M HCl was added to achieve a soil-to-solution ratio of 1:10 w/w. The resulting suspension was periodically stirred for 6 h, left overnight, the supernatant was separated by decantation. The decalcified soil was neutralized by 1 M NaOH to a pH of 7.0, then 0.1 M NaOH was added to achieve a soil-to-solution ratio of 1:10 w/w. The suspension was stirred periodically for 6 h and left overnight. After 24 h, alkaline extraction began, the supernatant was separated by decantation and centrifugation (5 min at 3000 rpm). The alkaline extract of HS was separated from fulvic acids by precipitation, acidification of the solution of 6 M HCl to a pH of 1.0–2.0, and centrifugation. HS precipitate was again dissolved in a minimum volume of 0.1 M KOH, KCl was added (up to a potassium concentration of 0.3 M) for coagulation of finely dispersed mineral particles. The precipitate was separated by centrifugation. Next, the HS solution was treated with 0.1 M HCl + 0.3 M HF to precipitate and remove silicon-containing and other impurities. The resulting HS suspension was purified by dialysis, dried on a rotary vacuum evaporator at 40 °C, transferred to a glass crucible, and kept in the dark.

2.3. FTIR Instrumentation and Analysis

Fourier transform infrared (FTIR) spectra of humic substances were recorded on a single-beam Vertex 70 IR Fourier spectrometer (Bruker Optik GmbH, Ettlingen, Germany) equipped with a default MIR globar, a KBr beamsplitter, a room-temperature DLaTGS detector, and a GladiATR^{TM} single reflection attenuated total internal reflection (ATR) accessory with a diamond crystal (Pike Technologies, Madison, WI, USA). The following measurement conditions were used: spectral range, 4000–400 cm^{-1}; spectral resolution,

2 cm^{-1}; aperture, 8 mm; scanner velocity, 10 kHz; sample and background scan numbers co-added and averaged, 128; the double-sided, forward–backward acquisition mode was used. A background signal was recorded prior to each new sample; the baseline was not corrected during measurements. The spectrometer and accessories were continuously purged with –70 °C dew point air (a PG28L Purge Gas Generator, PEAK Scientific, Glasgow, United Kingdom) at 500 L/h. The sample was in the ambient atmosphere during the measurement. The environmental temperature was kept at 23 ± 1 °C by an air conditioner.

A small amount of the HS sample was placed on the ATR crystal surface and pressed with an ATR screw by a default protocol (screw click stop at maximum, the maximum pressure by the manufacturer, 30,000 psi).

Continuous heating was performed from 25 °C to 215 °C, heating rate, 0.25 °C/min; FTIR measurements were started at 25 °C at the start of the heating program and then with a step of Δ2.5 °C; the temperature at the beginning and the end of each measurement differed by no more than 1 °C. After heating to 215 °C, the sample was cooled back to 25 °C without delay with the same temperature program; the measurements were made at 215 °C and then with a step of Δ2.5 °C; the temperature at the beginning and the end of each measurement differed by no more than 1 °C. An empty ATR crystal signal was recorded under the same heating/cooling conditions as a background.

All the obtained data were processed by Bruker OPUS 8.5 software (Bruker Optik GmbH, Ettlingen, Germany). Both heating and cooling sets and the empty-crystal sets were subjected to atmospheric correction. Next, a corrected empty-crystal background set was subtracted from sample sets as primary background correction. The resulting spectral matrices were separated into high-energy (4000–2000 cm^{-1}) and low-energy (2000–400 cm^{-1}) parts, and the extended ATR correction [47] was performed for these matrices (ATR crystal, diamond; radiation incidence angle, 45 degrees; number of ATR reflections, 1; and refractive index, 1.5). Next, a 13-point smoothing procedure was performed.

Band maxima positions were assessed by the standard band search method of the OPUS software (finding the *x*-position of the interpolated maximum or minimum). The intensity is the corresponding *y*-value of the interpolated maximum (sensitivity parameter, 0.1–20%; the higher the threshold is, the fewer band maxima are found). All other details are given in [39,48–50]. For integrated areas of the bands, the integration method B (OPUS software) was used: a straight line is drawn between the peaks of the two manually defined frequency limits and the area above this line is integrated.

2.4. ICP-AES Analysis

For microelement analysis, an inductively coupled plasma atomic emission spectrometer (ICP-AES 720, Agilent Technologies, Santa Clara, CA, USA) equipped with an axial quartz torch, an inner 1.8 mm diameter injector tube, a double-pass glass cyclonic spray chamber, a OneNeb nebulizer, a Trident Internal Standard Kit (Glass Expansion, Pocasset, MA, USA), and an SPS3 autosampler was used. Unless noted otherwise, all units were from Agilent Technologies (Santa Clara, CA, USA). Conditions of ICP–AES measurements are summed up in Table S1 (Supplementary materials). A Sc (20 mg L^{-1}) internal standard solution was added online (an orange/blue polyvinyl chloride pump tube) to increase the accuracy of measurements. Results were collected and processed with ICP Expert II software 2.0.5 (Agilent Technologies, Santa Clara, CA, USA). All lines were measured simultaneously (a MultiCal mode). Linear or quadratic functions were used for calibration. All other details were as described previously [46].

3. Results and Discussion

3.1. Soil HS Samples and Temperature Changes

Table 1 shows that the molar ratio of C/N in HS preparations (as min–max) ranges from 9.9 to 13.2 in soddy podzolic soil and 12.0 to 19.7 in chernozem, which characterizes a higher degree of maturity of the organic matter of chernozem, and a decrease in the content of its relatively unstable (aliphatic) components. At the same time, the H/C molar ratio

decreases, from 1.05 to 1.39 in soddy podzolic soil to 0.66 to 1.12 in chernozem. This change reflects an increase in the aromaticity of SOM in the latter [51,52].

The fact that in order to use standard samples of humic acids it is necessary to have their most complete characterization was shown back in 1993 [53]. It was demonstrated that the heterogeneity of the chemical composition of preparations associated with the variation in the composition of the organic matter of soils developed in different natural conditions [53]. For other main elements (Table 2), the content of sulfur, phosphorus, and most of the metals represented is higher in the preparation of HS of soddy podzolic soil than chernozem. At the same time, HS samples contain the same amount of silicon and nickel, and the concentration of copper was higher in chernozem.

Table 2. The amounts of major elements in HS from soil samples (n = 3, p = 0.95).

Sample	Amount, % *w*/*w*							
	Al	**Fe**	**Si**	**K**	**Na**	**Ca**	**S**	**P**
Soddy podzolic soil	0.025	0.205	0.025	0.074	0.024	0.034	0.453	0.300
Chernozem	0.007	0.051	0.026	0.136	0.019	0.032	0.239	0.142

The relatively high contents of titanium and zirconium in the HS sample preparations of humic acids are unexpected (Table 3), since for a long time it has been believed that these elements are characteristic of soil-forming rocks and practically do not change their mineralogical forms [54]. However, a large amount of data obtained by several researchers indicate that formations of stable complexes of zirconium with organic matter exist [55]. In particular, this may be a result of the interaction of metal ions with acid binding carboxyl and phenolic hydroxyl groups of SOM [56,57].

Table 3. The amounts of minor elements in HS from soil samples (n = 3, p = 0.95).

Sample	Amount, mg/kg								
	Ba	**Co**	**Cr**	**Cu**	**Mg**	**Mn**	**Ni**	**Ti**	**Zr**
Soddy podzolic soil	109	17.6	18	50	55	13	24.4	251	38.35
Chernozem	46	13.4	26	255	37	4.1	24.8	110	17.28

3.2. General Band Assignment

The temperature dependences of IR spectra of HS isolated from chernozem and soddy podzolic soils were studied upon continuous heating from 25 to 215 °C as this range matching the mild conditions with the minimum decomposition of SOM in soil samples [45]; the main process below 200 °C is dehydration [58]. Changes in the HS molecular framework start at higher temperatures: the polysaccharide decomposition, the elimination of functional groups, and destruction of phenolic compounds occur at 200–400 °C or higher temperatures [59]. However, a small contribution from SOM decomposition is also possible in the tested range of 25–215 °C [45], which was taken into account during the experiments in this study.

Temperature dependences of IR spectra of HS isolated from chernozem and soddy podzolic soils upon heating in the selected temperature range are shown in Figure 1. Band assignment is summed up in Table 4.

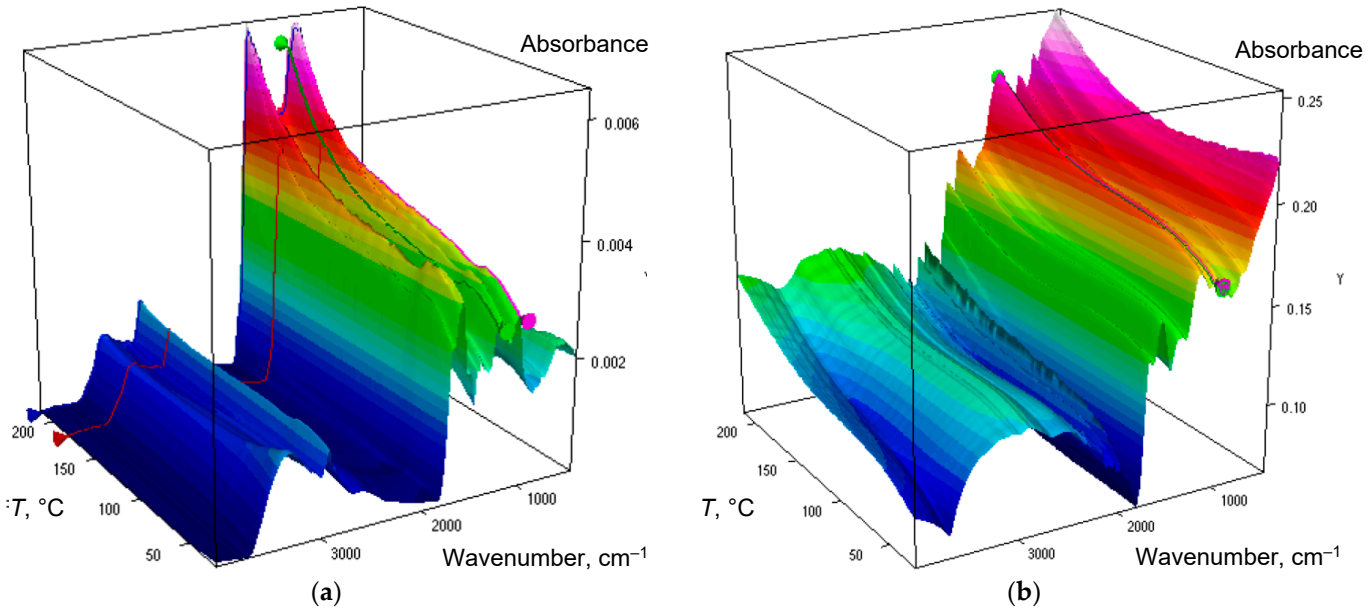


Figure 1. Temperature cube of information for IR spectra of humic substances isolated from (**a**) chernozem and (**b**) soddy podzolic soil.

Table 4. Major band assignment and thermal behavior for humic substance preparations isolated from studied soils.

Band Maximum *, cm^{-1}	Therm. Behavior of Integral Intensity **	SiO_2/Mineral/Water Constituents	Organic Constituents
3740–3600	=	Hydrogen-bond SiO–H ··· OH_2 stretch (amorph.) [60–62]	n/a
3490	↓	Water, liquid: asym. stretch v_3	O–H, phenolic, alcohol, carboxylic
3350	↓	Hydrogen-bonded SiO–H ··· H_2O SiO–H stretch (α-quartz) [60] water: v_1, v_3, and overt. of v_2	n/a
3270	↓	Water, liquid: sym. stretch v_1	O–H, phenolic, alcohol, carboxylic C=O ov.
→ **3130–3065**	= ***	n/a	C–H aromatic chain stretch
→ **3035–3030**	↑ ***	n/a	C–H aromatic chain stretch; C–H alkene chain stretch
← **2970–2960**	=	(?) SiO_2 overt.-comb. bands	C–H, CH_3 asym. stretch
← **2930–2910**	↑	(?) SiO_2, overt.-comb. bands	C–H, CH_2 asym. stretch [63–66]
← **2880**	=	n/a	C–H, CH_3 sym. stretch
← **2860–2850**	↓	n/a	C–H, CH_2 sym. stretch [63–66]
1845	↑	SiO_2 comb. band	C=O stretch
← **1790—1780**	↑	SiO_2 comb. band	C=O stretch
1775 (sh) Q	=	(?) SiO_2 comb. band	C=O stretch
→ **1740**	=	n/a	C=O stretch
1730—1700	↑	(?) SiO_2 comb. band	N–H bend, amine; alkene –C=C– stretch; substituted aromatics
1680 Q	=	SiO_2 comb. band	n/a
1670—1650	=***	Water, absorbed: bend v_2 [67]	**amide I**, aromatic –C=C– stretch [68]
1625	↓	H-bonded SiOH ··· OH_2 HO–H stretch [60] Water: bend v_2	N–H bend, C=O stretch, C=C stretch
1580 Q	=↓	SiO_2 overt.	C–C stretch, aromatic rings

Table 4. *Cont.*

Band Maximum *, cm^{-1}	Therm. Behavior of Integral Intensity **	SiO_2/Mineral/Water Constituents	Organic Constituents
← 1560	↑	n/a	Carboxylate, asym. stretch; (?) C=O stretch
← 1540—1510 Q	=↓	SiO_2 comb. band [69]	**amide II**, aromatic rings, carboxyl C
← 1460—1450	=	SiO_2 amorph. comb. band; carbonate [70]	O–H, C–H scissoring
→ 1420	↓	Mg–OH stretch [71]	C–O stretch
→ 1395—1375, triplet	=	SiO_2 comb. band [71] Water: O–H, coordinated bonded	Aromatic rings; carboxylate, sym. stretch; a comb. band of phenolic or COO stretch with CH_2 and CH_3 bands; non-carboxyl C–O–H in-plane bend [72]
→ 1360	↑	SiO_2 comb. band [71]	n/a
→ 1265	↑	SiO_2 comb. band	**amide III**, C–O stretch, aromatic rings and carboxylic acids [65], CH_2 rocking; C–N stretch
→ 1220—1210	↓	SiO_2 lattice [73]	n/a
1175 Q	↓	SiO_2 comb. band [71], amorph. [74]	CH_2 wagging
← 1153—1163 Q	↑	SiO_2 lattice [73]	C-O of carbohydrates; hydrogen-bonded stretching mode of C-OH groups; CH deformations [75–77]
→ 1120—1110	↑	amorph. silica [78]	n/a
← 1080 Q	↓	O–Si–O lattice stretch [73]	n/a
1070 Q	↓	SiO_2, (kaolinite, illite) O–Si–O lattice asym. stretch [73]	n/a
→ 1037 Q	↓	Silicate (kaolinite, illite) Si–O asym. stretch; Al–O stretch [70]	In plane C–H bend (non-aromatic) and carbohydrates; carboxyl out-of-plane C–O–H bend
1025—1000	= ***	SiO_2 Si–O stretch lattice	C–H bend (non-aromatic)
930–910 (sh)	↓	Silicate, aluminosilicate, ov. [74]	n/a
← 840–830	= ****	Al–OH (clay minerals), smectite, illite [79]; interfacial water librations [80]	cellulose
→ 796 Q	↓	SiO_2 silicate, lattice sym. Si–O–Si stretch [73,74]	Out of plane C–H bend (non-aromatic)
→ 775 Q	↓	α-quartz [73,78]	n/a
→ 750–730 (sh) (soddy podzolic)	↑	Mg–OH, Al–OH (clay minerals)	Polyaromatic [81] Out of plane C–H bend (aromatic); in-phase rock vibrations of C_{4+} alkanes [82]
→ 697 Q	=	SiO_2 Si–O–Si bend [73]	n/a
630–610 Q	=	Structural vibrations in quartz [83] Water: librations [80]	non-carboxylic, out-of-plane C–O–H bend; CH out-of-plane bending vibrations in biosystems [84]
535 Q	↑	α-quartz (?) [73] kaolinite	n/a
513 Q	=	silicate O–Si–O bend [73],	n/a
470 Q	=	SiO_2 O–Si–O bend [74]; O–Al–O [70]	n/a
450 Q	=	SiO_2 O–Si–O bend lattice [73,74]	C–C–C vibrations [85]
430–420 Q	=	Mg–OH, Al–OH (clay minerals)	C–C–C vibrations [85]

Notes: * The maximum is given as an average or a range; temperature-dependent frequency shift is marked bold with preceding arrows corresponding to a redshift (→) or a blueshift (←); "Q" means the intense band in the quartz spectra; (sh) means a shoulder. ** "↑" is an increase, "↓", a decrease, "=", no change; *** a decrease of intensity for $T > 200$ °C; **** an increase in intensity for $T > 200$ °C.

Subranges of the mid-IR range were selected considering their characteristics and methods of IR spectroscopy [39,48–50]. In this paper, we divided the mid-IR range

4000–400 cm^{-1} into six regions according to the previous study on HS of brown coal [39]: hydrogen-bond speciation region (4000–3100 cm^{-1}), CH-speciation region (3100–2800 cm^{-1}), quartz combination region (2800−1780 cm^{-1}), HSOM region (1780−1270 cm^{-1}), SiO_2 overtone region (1270–650 cm^{-1}), and quartz lattice region (650–400 cm^{-1}).

The hydrogen-bond speciation region is characterized by a broad band combining condensed-phase antisymmetric and symmetric hydrogen-bond bands at 3490–3270 cm^{-1}; below 120 °C, these bands are unresolved and centered at 3350 cm^{-1}. A series of low-intensity and poorly resolved bands at 3740–3600 cm^{-1} (Table 4) can be assigned to the stretch of hydrogen bonds in SiO–H $\cdots$ OH_2 (both crystalline and amorphous species) [60–62] but these bands are not well resolved due to spectral overlap with atmospheric water bands. Thus, they are excluded from the following consideration.

The CH-speciation region comprises low-to-medium-intensity bands at 3100–3060 cm^{-1}, alkene = CH_2, and aromatic sp^2 stretch [39], more pronounced with temperature; weak bands at 2970 and 2880 cm^{-1}, the stretch of methyl groups; and strong bands at 2920 and 2850 cm^{-1}, the antisymmetric and symmetric stretch of methylene groups (Figure S2, Supplementary Materials).

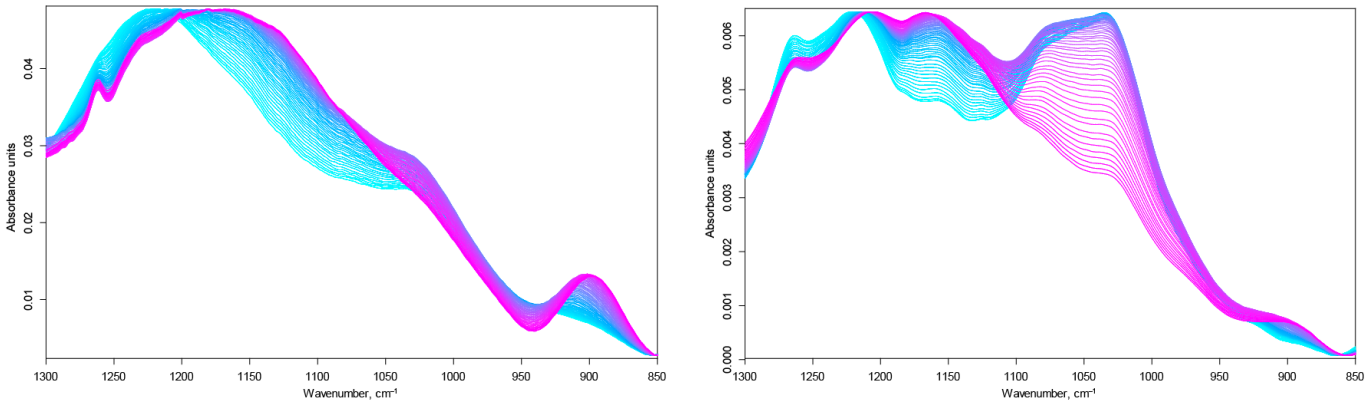
This region shows the band at 2650 cm^{-1} and weak bands of 2450 and 2407 cm^{-1}: they should be treated as artifact bands due to the contributions from the diamond ATR crystal (Figure S1, Supplementary Materials); thus, these bands are excluded from the further consideration. The overall picture is the same as in brown-coal HS [39], although the relative intensity of the bands of methyl groups is much lower in the case of soil HS. The region of 2500–2000 cm^{-1} has no specific bands, only artefact bands attributed to the residual ATR crystal absorption; thus, this region is excluded from consideration.

In the HSOM region, the major band at 1655−1645 cm^{-1}, a shoulder (Figure S3, Supplementary Materials), is the covalent bond bending (v_2) of absorbed liquid water [67]. The broader band at 1640−1610 cm^{-1} is free or slightly absorbed water, the maximum decrease in intensity is at 1640−1620 cm^{-1}. A series of low-intensity bands at 1850−1700 cm^{-1} are the C=O stretch of HS functional groups, and their structure is revealed during dehydration upon the temperature increase. The region at 1580−1510 cm^{-1} comprised of medium-to-low intensity bands (Figure S3, Supplementary Materials) is the antisymmetric carboxylate stretch of various acidic groups, with a possible contribution from SiO_2 overtones.

A band at 1400−1340 cm^{-1} (Figure S4, Supplementary Materials) is the corresponding symmetric carboxylate stretch [86]. Soddy podzolic soil and chernozem differ by the number of bands and the shape with a very high-intensity band at 1390 cm^{-1}. This may be attributed to high amounts of aliphatic compounds in soddy podzolic soil [87,88] confirmed by elemental-ratio data (Section 3.1, Table 1). The broad and relatively weak band at 1265−1260 cm^{-1} (Figure 2) is the C–O stretch, aromatic rings, and carboxylic acids of the Amide III range [65]; taking into account the character of the sample, the contribution from SiO_2 may be considered negligible.

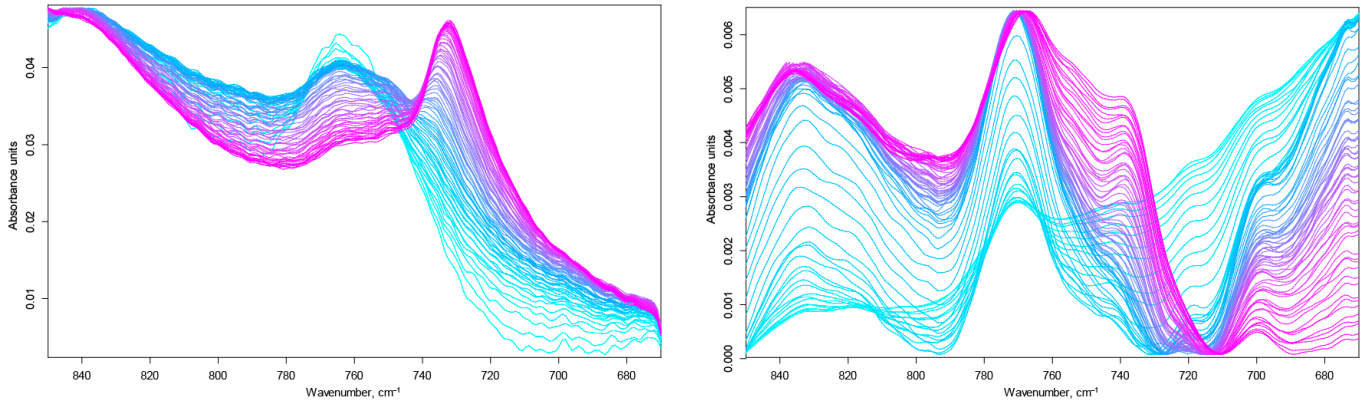
In the SiO_2 overtone region, the spectra for both soils from the viewpoint of appearing bands differ insignificantly (Figures 2 and 3). The main bands belong to 1230−1220 cm^{-1}, quartz lattice [48,73] (Figure 2); the broad band at 1120−1070 cm^{-1} is the O–Si–O stretch in both crystalline and amorphous SiO_2 species (Figure 2).

Other bands are 1035 cm^{-1} and low-intensity 1010 cm^{-1} (shoulder), amorphous SiO_2 O–Si–O stretch (not present in quartz); intense 912–900 cm^{-1}, amorphous silica [74]; 798 cm^{-1} (O–Si–O stretch) (shoulder); and 775 cm^{-1} (chernozem only). All quartz bands, even the most intense, 798 and 697 cm^{-1}, are weak in soddy podzolic HS and almost absent in chernozem HS samples due to a very high degree of purification from the matrix [40].



(**a**) (**b**)

Figure 2. Normalized ATR IR absorption spectra of humic substances from (**a**) chernozem and (**b**) soddy podzolic soil in the region 1300–850 cm^{-1} after ATR correction. Temperature increases from 25 to 215 °C, shown by blue to magenta lines.



(**a**) (**b**)

Figure 3. Normalized ATR IR absorption spectra of humic substances from (**a**) chernozem and (**b**) soddy podzolic soil in the region 850–670 cm^{-1} after ATR correction. Temperature increases from 25 to 215 °C, shown by blue to magenta lines.

Relatively weak bands, compared to SiO_2, at 830 and 750–740 cm^{-1} (Figure 3) belong to Al–OH [79]. Sevenfold higher intensities of these bands in soddy podzolic soil are well correlated with the amount of Al in these HS samples (Table 2).

In the lattice region (Figure S5, Supplementary Materials), most bands belong to the quartz lattice: medium-intensity 535 and 513 cm^{-1}, Si–O–Si bend; and 470, 450, and 430–420 cm^{-1}, O–Si–O bend [48,73,74]. Most bands, except for 470–450 cm^{-1}, are visible in the spectra of soddy podzolic soil only. A weak band at 670 cm^{-1} is the residual gaseous CO_2 band (doubly degenerate bend) excluded from further consideration.

3.3. Temperature Dependences of Band Maxima

The overall course of changes in IR spectra of HS from soddy podzolic and chernozem soils is illustrated by Figures 1 and S1 (Supplementary Materials). Figures 2 and 3 and Figures S2–S5 (Supplementary Materials) show spectra normalized by the maximum in the selected sub-regions to illustrate shifts of the band maxima.

The frequency shift is reversible and, when cooled, all the band maxima return to their original frequency, with very little deviation from the heating part (except for the water bands that reappear slower upon cooling compared to heating). In all the cases, the observed changes are summed up below.

In the region of hydrogen bonds (4000–3100 cm^{-1}), almost all the bands do not show a significant change in the frequencies of band maxima (Figure S1, Supplementary Materials); the value is no more than 0.5 cm^{-1} or ca. 0.01%, which should be considered a value significantly lower than the used spectral resolution. This behavior is similar to the previous findings with HS from brown coal [39]. The hydrogen continuum decreases (Figure 4) in the whole range 3600–3100 cm^{-1}, antisymmetric and symmetric parts cannot be reliably treated without band deconvolution and baseline correction, and the observed band does not experience redshifts or blueshifts.

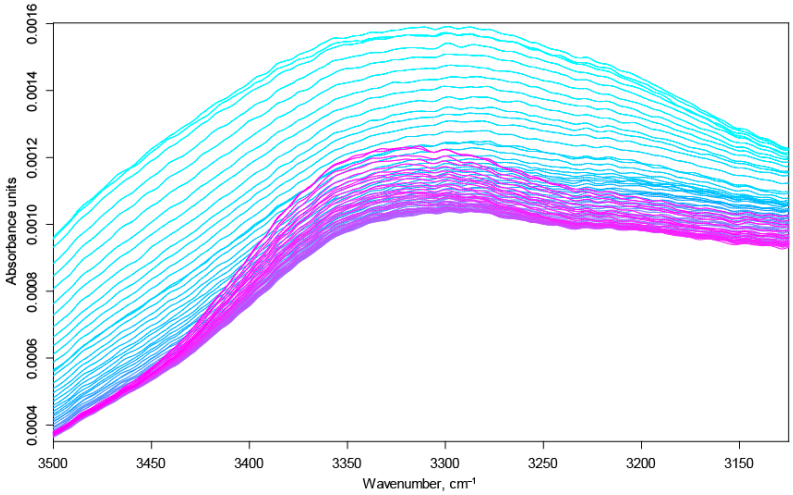


Figure 4. ATR IR absorption spectra of humic substances from soddy podzolic soil in the region 3500–3125 cm^{-1} after ATR correction. Temperature increases from 25 to 215 °C, shown by blue to magenta lines.

In the CH-speciation region (3100–2500 cm^{-1}), bands of 3130–3065 and 3035–3030 cm^{-1} assigned to the C–H aromatic chain or C–H alkene chain stretch show a redshift of –(1–2) cm^{-1}, while bands corresponding to C–H methylene alkane bands for both soil types show a blueshift of +(3–5) cm^{-1} (Figure 5).

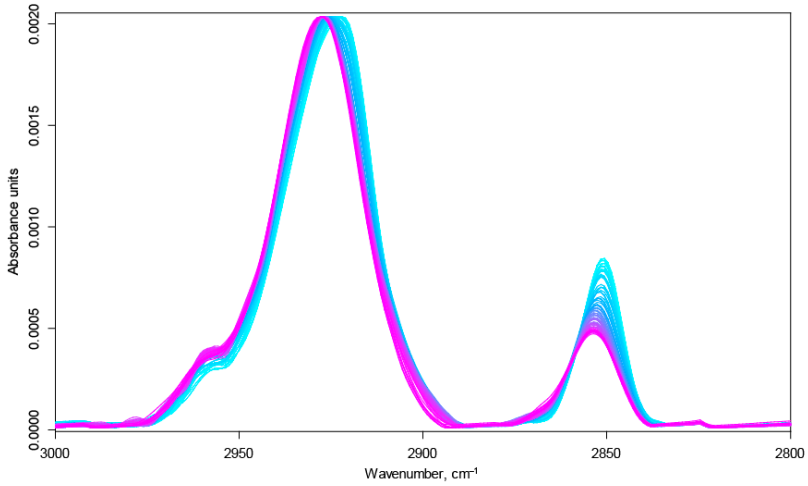


Figure 5. Normalized ATR IR absorption spectra of humic substances from soddy podzolic soil in the region 3000–2800 cm^{-1} after ATR correction and background correction. Temperature increases from 25 to 215 °C, shown by blue to magenta lines.

In the HSOM region (1780−1270 cm^{-1}), a distinct picture is revealed for both soils: bands probably correspond to quartz overtones (1845, 1790, and 1680 cm^{-1}) and do not show a maximum shift. The band at 1775 cm^{-1} shows a blueshift of +2 cm^{-1}. The band at

1460−1450 cm^{-1} also shows a slight blueshift (+0.5 cm^{-1}). The band of weakly absorbed water (1625 cm^{-1}) shows a redshift of –8 cm^{-1}. The absorbed water band at 1650 cm^{-1} experiences a blueshift (+0.5 cm^{-1}).

The bands at 1580−1560 cm^{-1} (antisymmetric carboxylate) experience a blueshift of +(2–3) cm^{-1} (0.2%), Figure 6a. The corresponding band at 1380 cm^{-1} (symmetric carboxylate) experiences a mirror-like redshift, Figure 6a, which is consistent with the literature data that for coupled vibrations, the energy of antisymmetric vibrations increases with temperature, while the energy of symmetric decreases [89]. This behavior is similar to coal HS [39]. As for brown coal HS [39], the behavior of bands at 1560 and 1380 cm^{-1} (symmetric carboxylate) and the high intensities of these bands imply that carboxylic groups are mainly carboxylates. It is noteworthy that the bands at 1780 and 1265 cm^{-1}, which can be assigned to the pair of carbonyl and C–OH bands in carboxylic acids, are much less intense, but show the same opposite behavior, a blueshift and a redshift, respectively, with almost the same amplitude (Figure 6b).

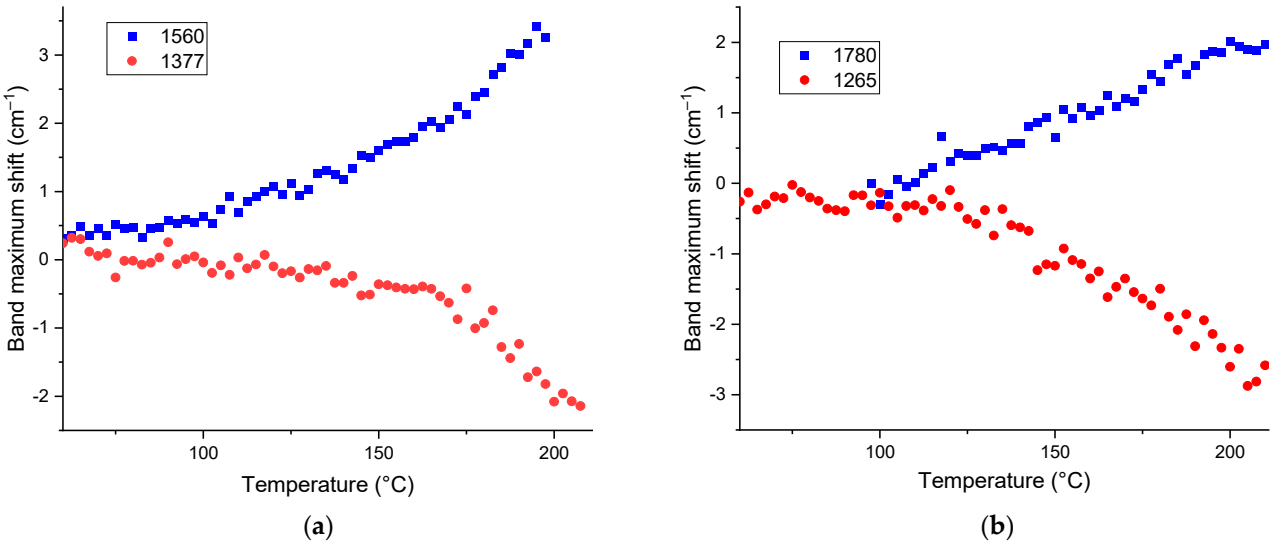


Figure 6. Temperature shifts in maximum positions corresponding to (**a**) carboxylate bands, 1560 and 1380 cm^{-1} and (**b**) carboxylic acid bands, 1780 and 1265 cm^{-1} for HS from soddy podzolic soil.

All other bands with SOM attribution (1420−1260 cm^{-1}) experience redshifts of –(1.5–2.5) cm^{-1} or 0.1–0.3%; the largest one is for 1265 cm^{-1}, Figure 7.

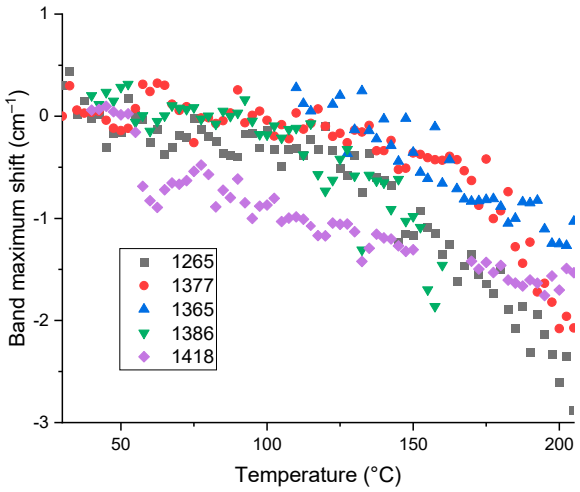


Figure 7. Temperature shifts in maximum positions corresponding to bands at 1265, 1365, 1377, 1386, and 1418 cm^{-1} for HS from soddy podzolic soil.

In the SiO_2 overtone region (1270–650 cm^{-1}), most bands can be attributed to lattice vibrations of residual quartz and other structured inorganic matrix components, and they show a redshift of −(2–5) cm^{-1} (0.6–0.7%). Bands at 770 and 745–740 cm^{-1} exhibit a redshift of −(3–5) cm^{-1} or (0.4–0.6)% (Figure 8a), which is smaller than for other bands as it does not belong to the quartz lattice frequencies but amorphous silica species. This confirms our previous findings with coal HS that these bands belong to other residual mineral species in HS samples [39] (Figure 8a), so that it can be the manifestation of SOM, in-phase rock CH_2 vibrations of C_4 or higher alkanes [82], like HS from brown coal.

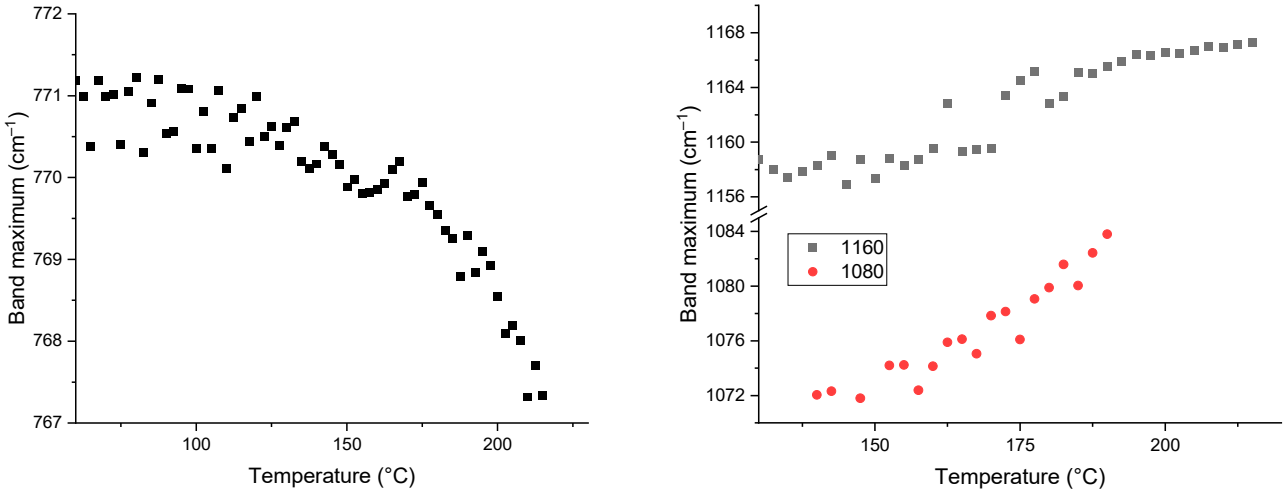


Figure 8. Temperature shifts in maximum positions of bands at (**a**) 770 cm^{-1} and (**b**) 1160 and 1080 cm^{-1} at temperatures over 110 °C for HS from soddy podzolic soil.

The band at 1070 cm^{-1} (O–Si–O lattice antisymmetric stretch [73]) is almost stable up to 130 °C, but at higher temperatures it shows a large blueshift, +10 cm^{-1} (Figure 8b). The same behavior is revealed for the weak band at 1163 cm^{-1} that can be attributed to lattice [90]; the temperature dependence does not correspond to quartz lattice changes. However, the behavior of this band is complex: a redshift by −10 cm^{-1} by heating to ca. 50 °C followed by a blueshift of the same amplitude to 150 °C (Figure 8b), which was found for HS of both soil types.

All other bands attributed to quartz show the temperature behavior not different from quartz samples [39] and do not differ for chernozem and soddy podzolic HS, which correlates with the same amount of Si in these samples (Table 3). Similar behavior is found for medium-to-low intensity bands attributed to quartz at 1035−1025, 910–990, and 840–830 cm^{-1}: a slight redshift of −(1–2) cm^{-1}.

In the region of fundamental SiO_2 vibrations (650–400 cm^{-1}), lattice vibrations of the matrix at 620, 540–535, and 510 cm^{-1} (Si–O–Si), 470, 450, 430, and 394 cm^{-1} (O–Si–O) do not show any shifts following the behavior of fundamental vibrations (Figure 9). The band at 697 cm^{-1} (as a counterpart of the lattice vibration at 354 cm^{-1} [73]) shows a blueshift of +3 cm^{-1}, which agrees well with the thermal behavior of this band for brown-coal HS [39].

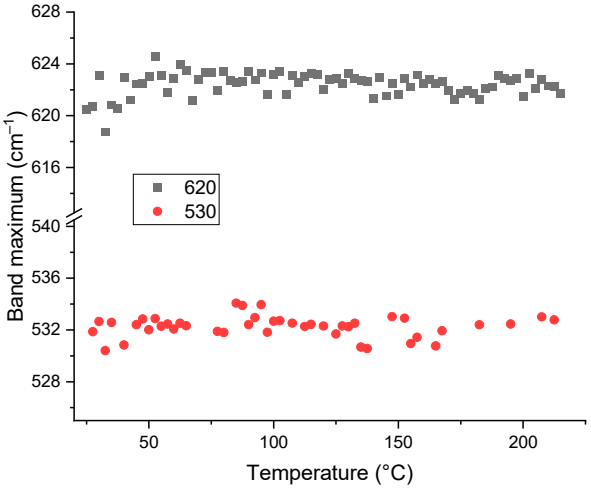


Figure 9. Plot of spectral positions (wavenumbers at maxima, cm^{-1}) for the bands at 620 and 530 cm^{-1} corresponding to skeletal vibrations of quartz for HS from soddy podzolic soil as a function of temperature.

3.4. Temperature Dependences of Band Intensities

Despite the characteristic behavior of band maxima (Section 3.3), the intensities at maxima show relatively high deviation resulting from the individual character of each spectrum (Figure S1, Supplementary Materials). On the contrary, band integration, over 5 to 20 cm^{-1} around the maximum depending on the band width, provides more reliable results. Thus, we used only the integrated areas of all the bands for their analysis.

In the region of the quartz matrix, such integration also results in a more informative analysis, as it provides better linearity of dependences for both the matrix bands and the bands responsible for SOM and other non-matrix components (see below).

The selected temperature range of 25 to 215 °C corresponds to the mild conditions with the minimum decomposition of SOM in soil samples. Still, the behavior of the majority of intensity curves for the selected bands shows that the whole studied range can be divided into three ranges (Figure 10).

The first part is the range of 25–60 °C, which is characterized by liquid water evaporation and relatively distinct changes in band intensities and maximum positions. The second part is the range from 60 to 180 °C, the high-temperature range, which is characterized by the change in the slope. The third part is the final subrange of 180 to 215 °C, which shows some changes in the behavior of bands corresponding mainly to SOM due to partial decomposition [45].

The bands corresponding to acidic groups show an increase in the intensity and the same behavior for both antisymmetric and symmetric bands (Figure 10a–e). Amide bands (1265 and 1510 cm^{-1}) have the same amplitude and behavior. Soddy podzolic soil shows more difference between these bands compared to chernozem (Figure 10). On the contrary, the band at 1630 cm^{-1} (water) shows an opposite behavior, a decrease over the whole studied range, which is quite similar by the scale for both HS samples (Figure 10f). For soddy podzolic soil, three stages can be seen: up to 60 °C with the highest slope, and 60−180 °C, with a slower decrease equal to the decrease for chernozem. Over 180 °C, there is no decrease for soddy podzolic HS, while chernozem HS retains the same slope.

It is noteworthy that the intensity of the carboxylate pair of bands, 1560 and 1380 cm^{-1}, is higher for soddy podzolic soil, while the intensities of non-dissociated carboxylic vibrations at 1780 and 1260 cm^{-1} are higher for chernozem. This correlates with the overall higher content of metals in soddy podzolic soil compared to chernozem HS (Tables 2 and 3).

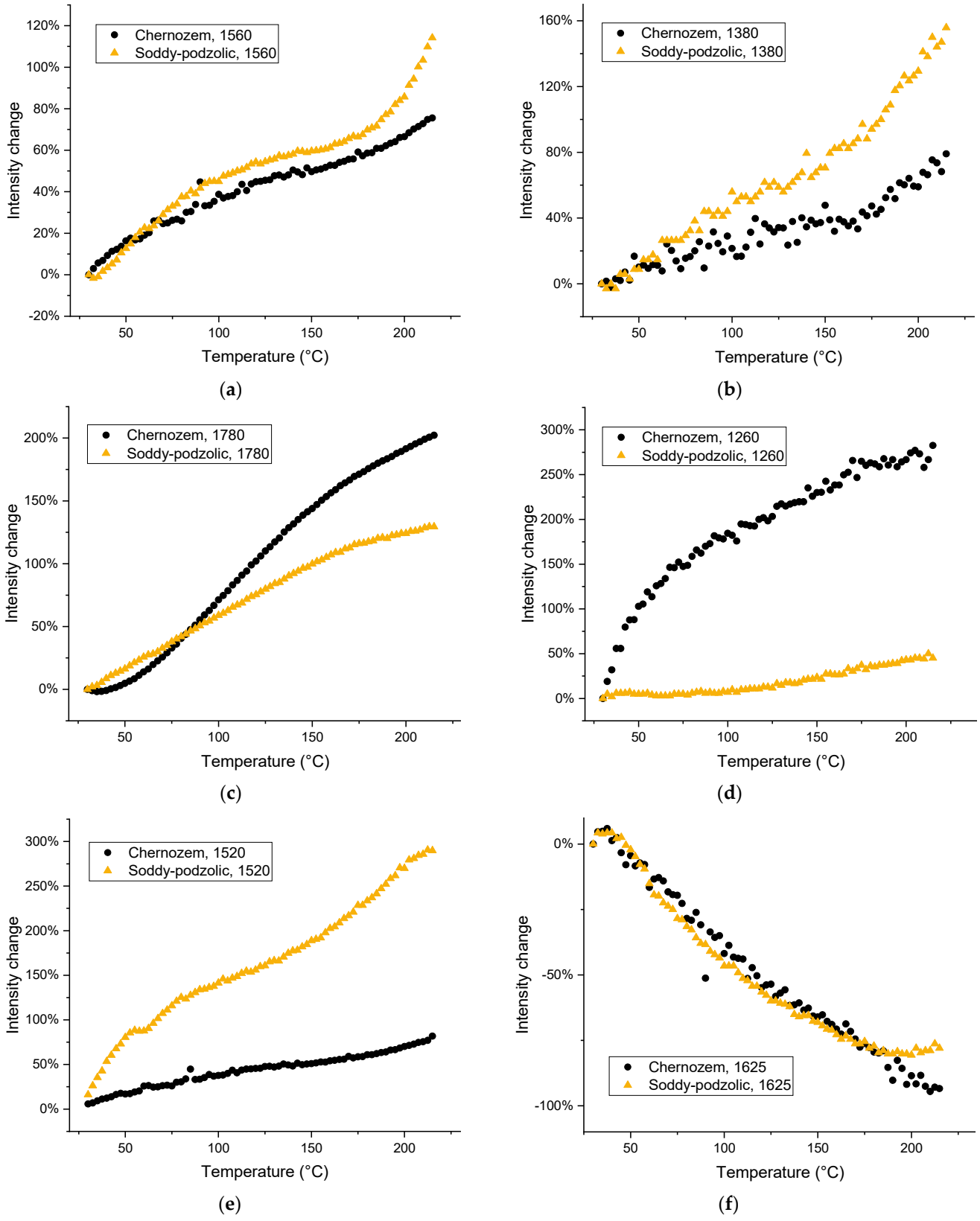
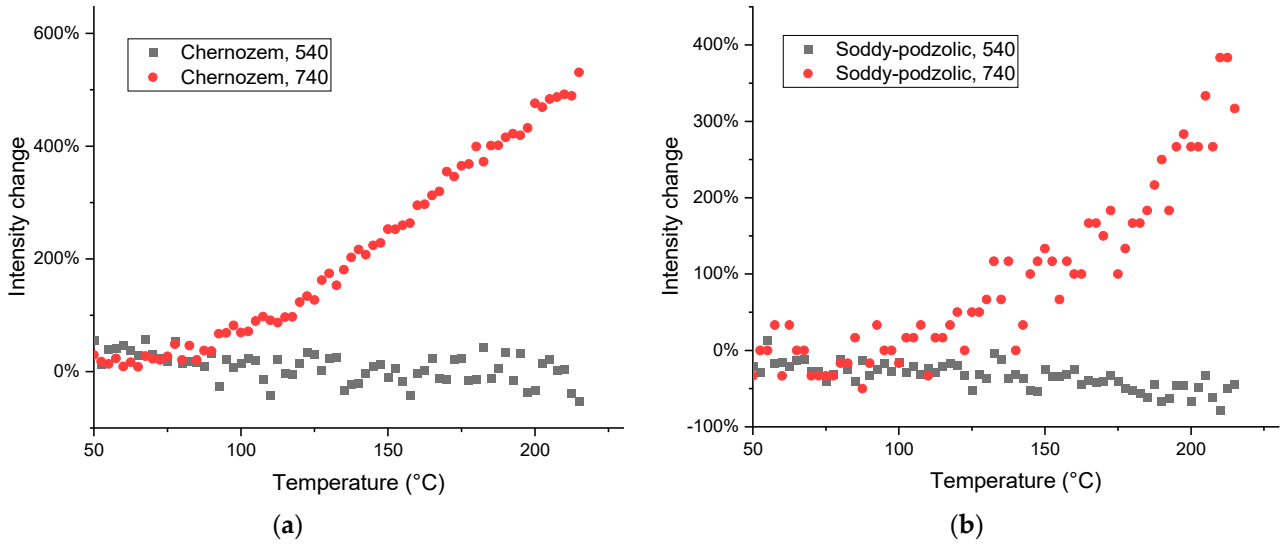


Figure 10. Thermal behavior of band intensities: (**a**) 1560; (**b**) 1380; (**c**) 1780; (**d**) 1260; (**e**) 1520; and (**f**) 1630 cm^{-1} for HS from chernozem (black dots) and soddy podzolic soil (light brown triangles).

It is noteworthy that the relative intensities of bands assigned to SOM increase significantly, while the intensities of bands attributed to SiO_2 do not change over the course

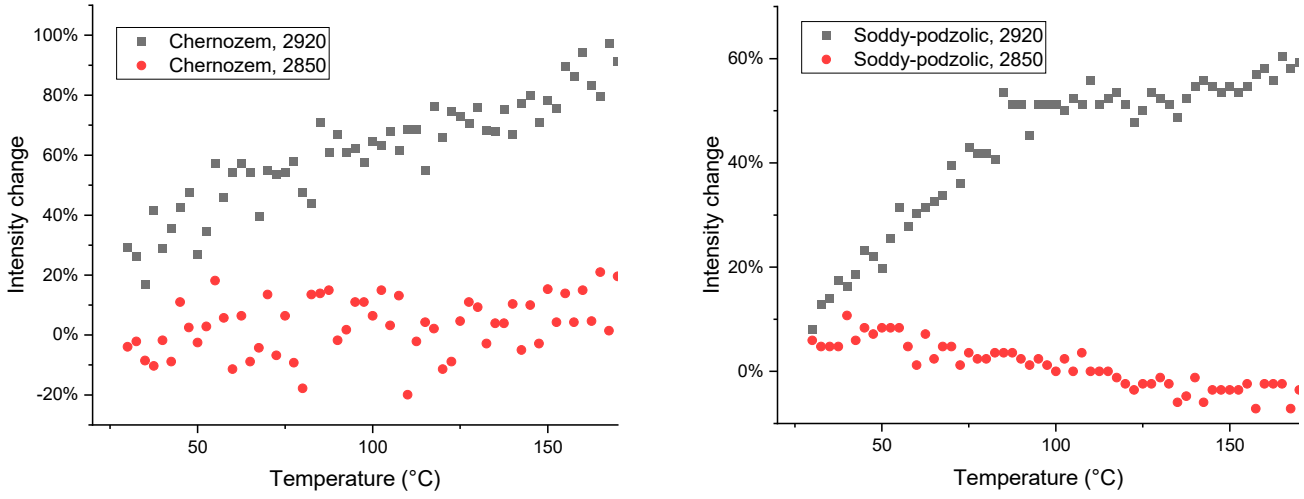
of heating (Figure 11 and Figure S6, Supplementary Materials). The large increase in intensity for the band at 748–732 cm^{-1} (the out-of-plane aromatic or polyaromatic C–H bend [81,82]) for both HS types is due to a decrease in the contribution from water to the background absorption, which hides this band at low temperatures and completely reveals this band at temperatures over 105 °C (Figure 3). The band intensity decreases in the same way upon cooling. The bands corresponding to water expectedly decrease in intensity (Table 4). The intensities of HSOM bands of methylene groups increase by 80−100%, for the functional-group range, and by 300–400% relative to the value at 105 °C (Figure 11).



(**a**) (**b**)

Figure 11. Thermal behavior of the integrated intensities of bands (**a**) 750 (red line) and 540 cm^{-1} (black line) for HS from (**a**) chernozem and (**b**) soddy podzolic soil.

For the bands corresponding to both HSOM and residual SiO_2, dependences of integral intensities of the same bands in chernozem and soddy podzolic HS show similar behavior. This is correct for CH_2 bands (3000–2800 cm^{-1}), the main bands in HSOM region (Figure 12) and in the subranges with band attribution to the SiO_2 matrix (Figure 11). Changes in the intensities of bands corresponding to SOM contributions are manifested in some cases significantly stronger in soddy podzolic soil compared to chernozem (Figure 12a,b).



(**a**) (**b**)

Figure 12. Thermal behavior of the integrated intensities of bands in the CH stretching region: (**a**) 2850 (red line) and 2920 cm^{-1} (black line) for HS from (**a**) chernozem and (**b**) soddy podzolic soil.

Bands that may be attributed to polyaromatic compounds [81], 750–720 cm^{-1} (Figure 11) show the growth, while out-of-plane vibrations of C–H aromatic structures and coupled C–H wagging vibrations of alkanes and alkenes at 715–700 cm^{-1} [82] and C–C–C bend vibrations of 450–425 cm^{-1} [85] in soddy podzolic soil show no change or drop in intensity, cf. a similar behavior of the bands in corresponding regions of the spectrum in quartz (Figure 13a).

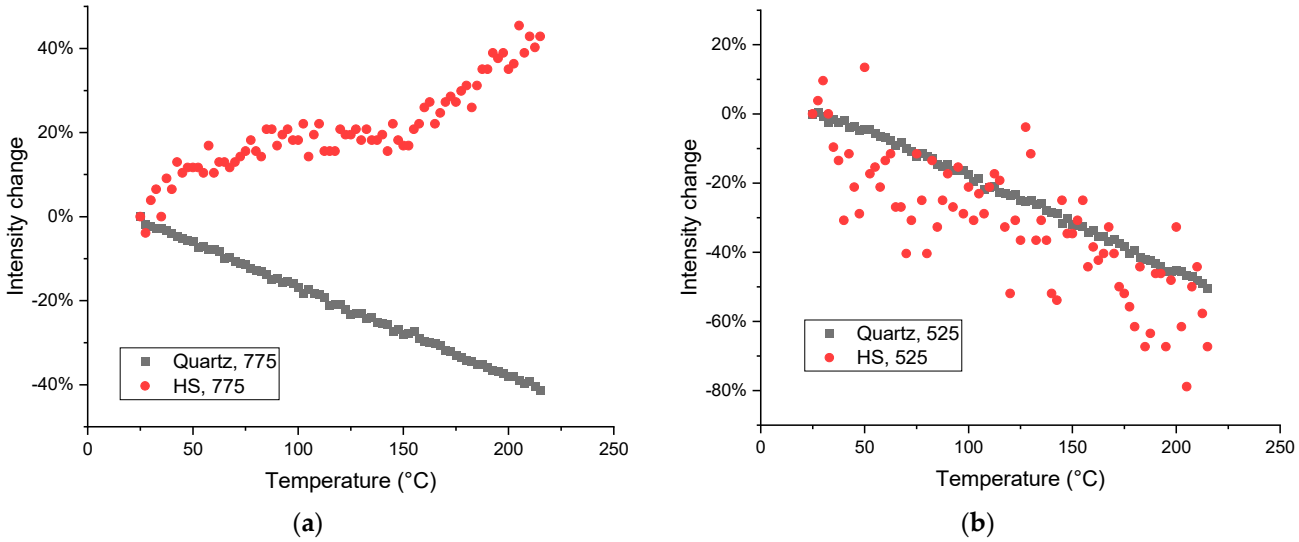


Figure 13. Thermal behavior of the integrated intensities of bands of (**a**) 775 and (**b**) 525 cm^{-1} in quartz (dark gray squares) and HS isolated from soddy podzolic soil (red dots). The high deviations in the case of the band at 525 cm^{-1} in humic substance sample is due to the very low intensity of this band (a low concentration compared to pure quartz).

In the case of a band of quartz without any contribution from organic matter, the behavior in HS and quartz is the same (Figure 13b); much worse reproducibility in soil HS is due to low amounts of quartz is the separated HS sample (Table 2).

Similar behavior indicates that these bands are probably caused by vibrations of the same type, coupled skeletal. In contrast to the intensities at the maximum absorption bands, the integral indicators are significantly more pronounced in chernozem compared to soddy podzolic soil. Thus, for the whole studied spectral region, we can ponder the bands at 1580−1560, 1410−1360, 1180−1160, and 1090−1080 cm^{-1}, as well as 875 and 750–720 cm^{-1} as mainly or mostly due to the soil organic matter, while contributions of SOM to 715–700 and 450–425 cm^{-1} are doubtful.

As a summary for all the samples, for all studied bands in the region of 1800–400 cm^{-1} and HS of both soil types, the bands of the quartz matrix experience a significantly smaller change in intensity than the bands assigned to organic matter (Figures 10 and 11). At the same time, the change in intensity for SiO_2 is almost linear (Figures 11 and 13), while SOM bands or bands having a SOM contribution experience growth for the entire selected temperature range with a large slope, and it intensifies in the temperature range over 150−160 °C (Figures 10 and 11).

Thus, when heated in air in the moderate temperature range of 25–215 °C, HS isolated from chernozem and soddy podzolic soil show different changes in IR spectral behavior both in the change in the wavenumber corresponding to the band maxima and the integrated band intensities. These trends provide more reliable identification of the character of the band compared to a single spectrum at a given temperature. Both the band shift scale and the various band dependence on temperature differ significantly for HSOM and residual inorganic matrix compounds. The bands corresponding to carboxylic and carboxylate groups demonstrate almost the same temperature-induced changes when comparing the samples. The different behavior of the lattice vibrations of quartz and organic matter

was found for chernozem and soddy podzolic HS, which is consistent with the different nature of SOM (mainly aromatic and aliphatic, respectively) and element analysis.

4. Conclusions

The temperature dependences of the maximum wavenumber positions (or shifts with temperature) in the IR spectrum and integral areas of the bands of soil HS samples in the range of moderate temperatures of 25–215 °C are signals that are more resistant to changes in the experimental conditions than the maxima and intensities of these bands at a single temperature. They can be used for better band attribution to SOM, matrix, or mixed bands and show different behavior for HS from soils of different types. The findings of this paper for humic substances separated from other components can be used for more detailed information on unseparated soil samples. Furthermore, these data may be used as a basis for comparison with other humic substances and humic-like substances both in qualitative analysis and quantifications.

Supplementary Materials: The following supporting information can be downloaded at https://www.mdpi.com/article/10.3390/agronomy13071740/s1. Table S1: Measurement parameters of soil humic substance samples by ICP–AES; Figure S1: Normalized ATR IR absorption spectra of humic substances from (a) chernozem, before the application of ATR correction and (b) soddy podzolic soil, after the application of ATR correction; in the region 4000–4000 cm^{-1}. Temperature increases from 25 to 215 °C, shown by blue to magenta lines; Figure S2: Normalized ATR IR absorption spectra of humic substances from (a) chernozem and (b) soddy podzolic soil in the region 3000–2750 cm^{-1} after ATR correction. Temperature increases from 25 to 215 °C, shown by blue to magenta lines; Figure S3: Normalized ATR IR absorption spectra of humic substances from (a) chernozem and (b) soddy podzolic soil in the region 1800–1450 cm^{-1} after ATR correction. Temperature increases from 25 to 215 °C, shown by blue to magenta lines; Figure S4: Normalized ATR IR absorption spectra of humic substances from (a) chernozem and (b) soddy podzolic soil in the region 1470–1320 cm^{-1} after ATR correction. Temperature increases from 25 to 215 °C, shown by blue to magenta lines; Figure S5: Normalized ATR IR absorption spectra of humic substances from (a) chernozem and (b) soddy podzolic soil in the region 600–400 cm^{-1} after ATR correction. Temperature increases from 25 to 215 °C, shown by blue to magenta lines; Figure S6: Thermal behavior of the integrated intensity of band of 697 cm^{-1} for HS from soddy podzolic soil.

Author Contributions: Conceptualization, M.A.P.; methodology, D.S.V. and O.B.R.; formal analysis, M.A.P., O.B.R. and D.S.V.; investigation, D.S.V. and O.B.R.; resources, D.S.V.; data curation, D.S.V.; writing—original draft preparation, M.A.P.; writing—review and editing, M.A.P., D.S.V. and O.B.R.; visualization, D.S.V.; supervision, M.A.P.; project administration, M.A.P.; funding acquisition, M.A.P. All authors have read and agreed to the published version of the manuscript.

Funding: This work was supported by the Russian Science Foundation, grant no. 19-13-00117.

Data Availability Statement: Not applicable.

Acknowledgments: This research was performed according to the Development program of the Interdisciplinary Scientific and Educational School of Lomonosov Moscow State University, "The future of the planet and global environmental change".

Conflicts of Interest: The authors declare no conflict of interest.

References

1. Malcolm, R.L. The uniqueness of humic substances in each of soil, stream and marine environments. *Anal. Chim. Acta* **1990**, *232*, 19–30. [CrossRef]
2. Kulikova, N.A.; Perminova, I.V. Interactions between Humic Substances and Microorganisms and Their Implications for Nature-like Bioremediation Technologies. *Molecules* **2021**, *26*, 2706. [CrossRef]
3. Stevenson, F.J. *Humus Chemistry: Genesis, Composition, Reactions*; Wiley: New York, NY, USA, 1994.
4. Perminova, I.V.; Garcia-Mina, J.M.; Podgorski, D.C.; Cervantes, F.J.; Efremenko, E.N.; Domingo, J.L. Humic substances and living systems: Impact on environmental and human health. *Environ. Res.* **2021**, *194*, 110726. [CrossRef] [PubMed]
5. Wang, S.; Zhang, Z.; Yin, X.; Wang, N.; Chen, D. Influences of Nitrogen Application Levels on Properties of Humic Acids in Chernozem Amended with Different Types of Organic Materials. *Sustainability* **2019**, *11*, 5405. [CrossRef]

6. Pukalchik, M.; Kydralieva, K.; Yakimenko, O.; Fedoseeva, E.; Terekhova, V. Outlining the Potential Role of Humic Products in Modifying Biological Properties of the Soil—A Review. *Front. Environ. Sci.* **2019**, *7*, 10. [CrossRef]
7. Trckova, M.; Matlova, L.; Hudcova, H.; Faldyna, M.; Zraly, Z.; Dvorska, L.; Beran, V.; Pavlik, I. Peat as a feed supplement for animals: A literature review. *Vet. Med.* **2005**, *50*, 361–377. [CrossRef]
8. Peña-Méndez, E.M.; Havel, J.; Patočka, J. Humic substances—Compounds of still unknown structure: Applications in agriculture, industry, environment, and biomedicine. *J. Appl. Biomed.* **2005**, *3*, 13–24. [CrossRef]
9. de Melo, B.A.; Motta, F.L.; Santana, M.H. Humic acids: Structural properties and multiple functionalities for novel technological developments. *Mater. Sci. Eng. C Mater. Biol. Appl.* **2016**, *62*, 967–974. [CrossRef]
10. Gašparovič, M.; Hrnčár, C.; Gálik, B. The effect of feed additives in pheasants fattening: A review. *J. Cent. Eur. Agric.* **2017**, *18*, 749–761. [CrossRef]
11. Pandey, A.K.; Pandey, S.D.; Misra, V.; Devi, S. Role of humic acid entrapped calcium alginate beads in removal of heavy metals. *J. Hazard. Mater.* **2003**, *98*, 177–181. [CrossRef]
12. Nardi, S.; Pizzeghello, D.; Muscolo, A.; Vianello, A. Physiological effects of humic substances on higher plants. *Soil Biol. Biochem.* **2002**, *34*, 1527–1536. [CrossRef]
13. Plyatsuk, L.; Chernysh, Y.; Ablieieva, I.; Bataltsev, Y.; Vaskin, R.; Roy, I.; Yakhnenko, E.; Roubík, H. Modelling and development of technological processes for low rank coal bio-utilization on the example of brown coal. *Fuel* **2020**, *267*, 117298. [CrossRef]
14. Skripkina, T.S.; Bychkov, A.L.; Tikhova, V.D.; Lomovsky, O.I. Mechanochemical Solid-Phase Reactions of Humic Acids from Brown Coal with Sodium Percarbonate. *Solid Fuel Chem.* **2019**, *52*, 356–360. [CrossRef]
15. Acharya, B.; Sule, I.; Dutta, A. A review on advances of torrefaction technologies for biomass processing. *Biomass Convers. Biorefin.* **2012**, *2*, 349–369. [CrossRef]
16. Winkler, J.; Ghosh, S. Therapeutic Potential of Fulvic Acid in Chronic Inflammatory Diseases and Diabetes. *J. Diabetes Res.* **2018**, *2018*, 5391014. [CrossRef] [PubMed]
17. Kononova, M.M. *Soil Organic Matter*, 2nd ed.; Elsevier: Amsterdam, The Netherlands, 1966. [CrossRef]
18. Huang, P.M.; Li, Y.; Sumner, M.E. (Eds.) *Handbook of Soil Sciences. Properties and Processes*, 2nd ed.; CRC Press: Boca Raton, FL, USA, 2012; p. 1436.
19. Gerke, J. The Central Role of Soil Organic Matter in Soil Fertility and Carbon Storage. *Soil Syst.* **2022**, *6*, 33. [CrossRef]
20. Plaza-Bonilla, D.; Álvaro-Fuentes, J.; Cantero-Martínez, C. Identifying soil organic carbon fractions sensitive to agricultural management practices. *Soil Tillage Res.* **2014**, *139*, 19–22. [CrossRef]
21. DeGryze, S.; Six, J.; Paustian, K.; Morris, S.J.; Paul, E.A.; Merckx, R. Soil organic carbon pool changes following land-use conversions. *Glob. Chang. Biol.* **2004**, *10*, 1120–1132. [CrossRef]
22. Kotzé, E.; Loke, P.F.; Akhosi-Setaka, M.C.; Du Preez, C.C. Land use change affecting soil humic substances in three semi-arid agro-ecosystems in South Africa. *Agric. Ecosyst. Environ.* **2016**, *216*, 194–202. [CrossRef]
23. Fultz, L.M.; Moore-Kucera, J.; Calderón, F.; Acosta-Martínez, V. Using Fourier-Transform Mid-Infrared Spectroscopy to Distinguish Soil Organic Matter Composition Dynamics in Aggregate Fractions of Two Agroecosystems. *Soil Sci. Soc. Am. J.* **2014**, *78*, 1940–1948. [CrossRef]
24. Ge, Y.; Thomasson, J.A.; Morgan, C.L.S. Mid-infrared attenuated total reflectance spectroscopy for soil carbon and particle size determination. *Geoderma* **2014**, *213*, 57–63. [CrossRef]
25. Tinti, A.; Tugnoli, V.; Bonora, S.; Francioso, O. Recent applications of vibrational mid-Infrared (IR) spectroscopy for studying soil components: A review. *J. Cent. Eur. Agric.* **2015**, *16*, 1–22. [CrossRef]
26. Linker, R. Application of FTIR Spectroscopy to Agricultural Soils Analysis. In *Fourier Transforms—New Analytical Approaches and FTIR Strategies*; Nikolic, G., Ed.; InTech: Tokyo, Japan, 2011; pp. 385–404. [CrossRef]
27. Viscarra Rossel, R.A.; Walvoort, D.J.J.; McBratney, A.B.; Janik, L.J.; Skjemstad, J.O. Visible, near infrared, mid infrared or combined diffuse reflectance spectroscopy for simultaneous assessment of various soil properties. *Geoderma* **2006**, *131*, 59–75. [CrossRef]
28. Roy, L. Quantitative FTIR analysis of paraben in finished dosage pharmaceuticals. *Abstr. Pap. Am. Chem. Soc.* **2013**, *246*, 1.
29. Celino, A.; Goncalves, O.; Jacquemin, F.; Freour, S. Qualitative and quantitative assessment of water sorption in natural fibres using ATR-FTIR spectroscopy. *Carbohydr. Polym.* **2014**, *101*, 163–170. [CrossRef]
30. Tanykova, N.; Petrova, Y.; Kostina, J.; Kozlova, E.; Leushina, E.; Spasennykh, M. Study of Organic Matter of Unconventional Reservoirs by IR Spectroscopy and IR Microscopy. *Geosciences* **2021**, *11*, 277. [CrossRef]
31. Artz, R.R.E.; Chapman, S.J.; Jean Robertson, A.H.; Potts, J.M.; Laggoun-Défarge, F.; Gogo, S.; Comont, L.; Disnar, J.-R.; Francez, A.-J. FTIR spectroscopy can be used as a screening tool for organic matter quality in regenerating cutover peatlands. *Soil Biol. Biochem.* **2008**, *40*, 515–527. [CrossRef]
32. Katon, J.E.; Phillips, D.B. Infrared Spectroscopy at Subambient Temperatures. *Appl. Spectrosc. Rev.* **1973**, *7*, 1–45. [CrossRef]
33. Zallen, R.; Conwell, E.M. The effect of temperature on libron frequencies in molecular crystals: Implications for TTF-TCNQ. *Solid State Commun.* **1979**, *31*, 557–561. [CrossRef]
34. Nanda, S.; Reddy, S.N.; Hunter, H.N.; Butler, I.S.; Kozinski, J.A. Supercritical Water Gasification of Lactose as a Model Compound for Valorization of Dairy Industry Effluents. *Ind. Eng. Chem. Res.* **2015**, *54*, 9296–9306. [CrossRef]
35. Sirotiak, M.; Bartošová, A. Changes in Structure and Content Humic Substances in Soil During the Laboratory Simulated Fires. *Trans. VŠB Tech. Univ. Ostrav. Saf. Eng. Ser.* **2016**, *11*, 42–48. [CrossRef]

36. Stevenson, F.J.; Goh, K.M. Infrared spectra of humic acids: Elimination of interference due to hygroscopic moisture and structural changes accompanying heating with KBr. *Soil Sci.* **1974**, *117*, 34–41. [CrossRef]
37. Zuyi, T.; Shifang, L.; Jianjun, Z.; Fenling, S. Studies of Thermal Transformations of Humic and Fulvic Acids in Soils I. Infrared Spectroscopy and Temperature-Programmed Pyrolysis Mass Spectrometry. *Chem. Ecol.* **1997**, *13*, 237–248. [CrossRef]
38. Kolokassidou, C.; Pashalidis, I.; Costa, C.N.; Efstathiou, A.M.; Buckau, G. Thermal stability of solid and aqueous solutions of humic acid. *Thermochim. Acta* **2007**, *454*, 78–83. [CrossRef]
39. Volkov, D.; Rogova, O.; Proskurnin, M. Temperature Dependences of IR Spectra of Humic Substances of Brown Coal. *Agronomy* **2021**, *11*, 1822. [CrossRef]
40. Kholodov, V.A.; Yaroslavtseva, N.V.; Konstantinov, A.I.; Perminova, I.V. Preparative yield and properties of humic acids obtained by sequential alkaline extractions. *Eurasian Soil Sci.* **2015**, *48*, 1101–1109. [CrossRef]
41. Ovchinnikova, M.F.; Orlov, D.S. Humus state of virgin and cultivated soils of the Chashnikovo experimental station. *Mosc. Univ. Soil Sci. Bull.* **1986**, *41*, 8–15.
42. Ivanov, V.V.; Vagner, M.V. On mineralogical composition of coarse loamy sod-podzol soils of Klinsko-Dmitrovskaya ridge near Chashnikovo. *Mosc. Univ. Soil Sci. Bull.* **1988**.
43. Semenyuk, O.V.; Telesnina, V.M.; Bogatyrev, L.G.; Benediktova, A.I.; Kuznetsova, Y.D. Assessment of Intra-Biogeocenotic Variability of Forest Litters and Dwarf Shrub–Herbaceous Vegetation in Spruce Stands. *Eurasian Soil Sci.* **2020**, *53*, 27–38. [CrossRef]
44. Cherkassov, G.N.; Masyutenko, N.P.; Gostev, A.V.; Pykhtin, I.G.; Zdorovtsov, I.P.; Akimenko, A.S. Long-Term Field Experiments On Chernozemic Soils Of Kursk Region, Russia. In Proceedings of the Soil Organic Matter Dynamics in Long-Therm Field Experiments and Their Modelling, Kursk, Russia, 14–17 September 2010; p. 35.
45. Volkov, D.S.; Rogova, O.B.; Proskurnin, M.A.; Farkhodov, Y.R.; Markeeva, L.B. Thermal stability of organic matter of typical chernozems under different land uses. *Soil Tillage Res.* **2020**, *197*, 104500. [CrossRef]
46. Karpukhina, E.A.; Vlasova, E.A.; Volkov, D.S.; Proskurnin, M.A. Comparative Study of Sample-Preparation Techniques for Quantitative Analysis of the Mineral Composition of Humic Substances by Inductively Coupled Plasma Atomic Emission Spectroscopy. *Agronomy* **2021**, *11*, 2453. [CrossRef]
47. Nunn, S.; Nishikida, K. Advanced ATR Correction Algorithm. In *Thermo Fisher Scientific Application Note*; Thermo Fisher Scientific: Waltham, MA, USA, 2008.
48. Krivoshein, P.K.; Volkov, D.S.; Rogova, O.B.; Proskurnin, M.A. FTIR photoacoustic spectroscopy for identification and assessment of soil components: Chernozems and their size fractions. *Photoacoustics* **2020**, *18*, 100162. [CrossRef] [PubMed]
49. Krivoshein, P.K.; Volkov, D.S.; Rogova, O.B.; Proskurnin, M.A. FTIR Photoacoustic and ATR Spectroscopies of Soils with Aggregate Size Fractionation by Dry Sieving. *ACS Omega* **2022**, *7*, 2177–2197. [CrossRef] [PubMed]
50. Volkov, D.; Rogova, O.; Proskurnin, M. Organic Matter and Mineral Composition of Silicate Soils: FTIR Comparison Study by Photoacoustic, Diffuse Reflectance, and Attenuated Total Reflection Modalities. *Agronomy* **2021**, *11*, 1879. [CrossRef]
51. Kurganova, I.N.; Lopes de Gerenyu, V.O.; Gallardo Lancho, J.F.; Oehm, C.T. Evaluation of the rates of soil organic matter mineralization in forest ecosystems of temperate continental, mediterranean, and tropical monsoon climates. *Eurasian Soil Sci.* **2012**, *45*, 68–79. [CrossRef]
52. Kurganova, I.N.; Telesnina, V.M.; Lopes de Gerenyu, V.O.; Lichko, V.I.; Karavanova, E.I. The Dynamics of Carbon Pools and Biological Activity of Retic Albic Podzols in Southern Taiga during the Postagrogenic Evolution. *Eurasian Soil Sci.* **2021**, *54*, 337–351. [CrossRef]
53. Qiang, T.; Xiao-quan, S.; Zhe-ming, N. Comparative characteristic studies on soil and commercial humic acids. *Fresenius J. Anal. Chem.* **1993**, *347*, 330–336. [CrossRef]
54. Kabata-Pendias, A. *Trace Elements in Soils and Plants*; CRC Press: Boca Raton, FL, USA, 2010.
55. Shahid, M.; Ferrand, E.; Schreck, E.; Dumat, C. Behavior and Impact of Zirconium in the Soil–Plant System: Plant Uptake and Phytotoxicity. In *Reviews of Environmental Contamination and Toxicology*; Whitacre, D.M., Ed.; Springer: New York, NY, USA, 2013; Volume 221, pp. 107–127. [CrossRef]
56. Oliva, P.; Viers, J.; Dupré, B.; Fortuné, J.P.; Martin, F.; Braun, J.J.; Nahon, D.; Robain, H. The effect of organic matter on chemical weathering: Study of a small tropical watershed: Nsimi-zoétélé site, cameroon. *Geochim. Cosmochim. Acta* **1999**, *63*, 4013–4035. [CrossRef]
57. Pokrovsky, O.S.; Schott, J. Iron colloids/organic matter associated transport of major and trace elements in small boreal rivers and their estuaries (NW Russia). *Chem. Geol.* **2002**, *190*, 141–179. [CrossRef]
58. Boguta, P.; Sokolowska, Z.; Skic, K. Use of thermal analysis coupled with differential scanning calorimetry, quadrupole mass spectrometry and infrared spectroscopy (TG-DSC-QMS-FTIR) to monitor chemical properties and thermal stability of fulvic and humic acids. *PLoS ONE* **2017**, *12*, e0189653. [CrossRef]
59. Chan, T.F.; Su, J.H.; Chung, Y.F.; Chang, H.L.; Yuan, S.S. Decreased serum leptin levels in women with uterine leiomyomas. *Acta Obstet. Gynecol. Scand.* **2003**, *82*, 173–176. [CrossRef] [PubMed]
60. Kronenberg, A.K. Chapter 4. Hydrogen Speciation and Chemical Weakening of Quartz. In *Silica*; De Gruyter: Berlin, Germany, 1994; pp. 123–176. [CrossRef]
61. Russell, J.D.; Fraser, A.R. Infrared methods. In *Clay Mineralogy: Spectroscopic and Chemical Determinative Methods*; Wilson, M.J., Ed.; Springer: Dordrecht, The Netherlands, 1994; pp. 11–67. [CrossRef]

62. Madejová, J. Baseline Studies of the Clay Minerals Society Source Clays: Infrared Methods. *Clays Clay Miner.* **2001**, *49*, 410–432. [CrossRef]
63. Calderón, F.J.; Mikha, M.M.; Vigil, M.F.; Nielsen, D.C.; Benjamin, J.G.; Reeves, J.B. Diffuse-Reflectance Mid-infrared Spectral Properties of Soils under Alternative Crop Rotations in a Semi-arid Climate. *Commun. Soil Sci. Plant Anal.* **2011**, *42*, 2143–2159. [CrossRef]
64. Calderón, F.J.; Reeves, J.B.; Collins, H.P.; Paul, E.A. Chemical Differences in Soil Organic Matter Fractions Determined by Diffuse-Reflectance Mid-Infrared Spectroscopy. *Soil Sci. Soc. Am. J.* **2011**, *75*, 568–579. [CrossRef]
65. Changwen, D.; Jing, D.; Jianmin, Z.; Huoyan, W.; Xiaoqin, C. Characterization of Greenhouse Soil Properties Using Mid-infrared Photoacoustic Spectroscopy. *Spectrosc. Lett.* **2011**, *44*, 359–368. [CrossRef]
66. Changwen, D.; Jianmin, Z.; Goyne, K.W. Organic and inorganic carbon in paddy soil as evaluated by mid-infrared photoacoustic spectroscopy. *PLoS ONE* **2012**, *7*, e43368. [CrossRef]
67. Max, J.J.; Chapados, C. Isotope effects in liquid water by infrared spectroscopy. III. H_2O and D_2O spectra from 6000 to 0 cm^{-1}. *J. Chem. Phys.* **2009**, *131*, 184505. [CrossRef]
68. Du, C.; Goyne, K.W.; Miles, R.J.; Zhou, J. A 1915–2011 microscale record of soil organic matter under wheat cultivation using FTIR-PAS depth-profiling. *Agron. Sustain. Dev.* **2013**, *34*, 803–811. [CrossRef]
69. Tan, C.Z. Optical interference in overtones and combination bands in α-quartz. *J. Phys. Chem. Solids* **2003**, *64*, 121–125. [CrossRef]
70. Nguyen, T.T.; Janik, L.J.; Raupach, M. Diffuse reflectance infrared fourier transform (DRIFT) spectroscopy in soil studies. *Soil Res.* **1991**, *29*, 49–67. [CrossRef]
71. Hofmeister, A.M.; Bowey, J.E. Quantitative Infrared Spectra of Hydrosilicates and Related Minerals. *Mon. Not. R. Astron. Soc.* **2006**, *367*, 577–591. [CrossRef]
72. Asselin, M.; Sandorfy, C. Anharmonicity and Hydrogen Bonding. The in-plane OH Bending and its Combination with the OH Stretching Vibration. *Can. J. Chem.* **1971**, *49*, 1539–1544. [CrossRef]
73. Spitzer, W.G.; Kleinman, D.A. Infrared Lattice Bands of Quartz. *Phys. Rev.* **1961**, *121*, 1324–1335. [CrossRef]
74. Bock, J.A.N.; Su, G.-J. Interpretation of the Infrared Spectra of Fused Silica. *J. Am. Ceram. Soc.* **1970**, *53*, 69–73. [CrossRef]
75. Fung, M.F.K.; Senterman, M.K.; Mikhael, N.Z.; Lacelle, S.; Wong, P.T.T. Pressure-tuning fourier transform infrared spectroscopic study of carcinogenesis in human endometrium. *Biospectroscopy* **1998**, *2*, 155–165. [CrossRef]
76. Wang, H.P.; Wang, H.C.; Huang, Y.J. Microscopic FTIR studies of lung cancer cells in pleural fluid. *Sci. Total Environ.* **1997**, *204*, 283–287. [CrossRef] [PubMed]
77. Schulz, H.; Baranska, M. Identification and quantification of valuable plant substances by IR and Raman spectroscopy. *Vib. Spectrosc.* **2007**, *43*, 13–25. [CrossRef]
78. Koike, C.; Noguchi, R.; Chihara, H.; Suto, H.; Ohtaka, O.; Imai, Y.; Matsumoto, T.; Tsuchiyama, A. Infrared Spectra of Silica Polymorphs and the Conditions of Their Formation. *Astrophys. J.* **2013**, *778*, 60. [CrossRef]
79. Inoue, A.; Watanabe, T. Infrared Spectra of Interstratified Illite/Smectite from Hydrothermally Altered Tuffs (Shinzan, Japan) and Diagenetic Bentonites (Kinnekulle, Sweden). *Clay Sci.* **1989**, *7*, 263–275. [CrossRef]
80. Tong, Y.; Kampfrath, T.; Campen, R.K. Experimentally probing the libration of interfacial water: The rotational potential of water is stiffer at the air/water interface than in bulk liquid. *Phys. Chem. Chem. Phys.* **2016**, *18*, 18424–18430. [CrossRef]
81. Yu, H.-G.; Nyman, G. The Infrared and UV-Visible Spectra of Polycyclic Aromatic Hydrocarbons Containing (5,7)-Member Ring Defects: A Theoretical Study. *Astrophys. J.* **2012**, *751*, 3. [CrossRef]
82. Workman, J. *The Handbook of Organic Compounds, Three-Volume Set: NIR, IR, R, and UV-Vis Spectra Featuring Polymers and Surfactants*; Elsevier Science: Amsterdam, The Netherlands, 2000.
83. San Andrés, E.; del Prado, A.; Mártil, I.; González-Díaz, G.; Bravo, D.; López, F.J.; Fernández, M.; Bohne, W.; Röhrich, J.; Selle, B.; et al. Bonding configuration and density of defects of SiO_xH_y thin films deposited by the electron cyclotron resonance plasma method. *J. Appl. Phys.* **2003**, *94*, 7462–7469. [CrossRef]
84. Chiang, H.P.; Song, R.; Mou, B.; Li, K.P.; Chiang, P.; Wang, D.; Tse, W.S.; Ho, L.T. Fourier transform Raman spectroscopy of carcinogenic polycyclic aromatic hydrocarbons in biological systems: Binding to heme proteins. *J. Raman Spectrosc.* **1999**, *30*, 551–555. [CrossRef]
85. Schenzel, K.; Almlöf, H.; Germgård, U. Quantitative analysis of the transformation process of cellulose I → cellulose II using NIR FT Raman spectroscopy and chemometric methods. *Cellulose* **2009**, *16*, 407–415. [CrossRef]
86. Baes, A.U.; Bloom, P.R. Diffuse Reflectance and Transmission Fourier Transform Infrared (DRIFT) Spectroscopy of Humic and Fulvic Acids. *Soil Sci. Soc. Am. J.* **1989**, *53*, 695–700. [CrossRef]
87. Perminova, I.V.; Shirshin, E.A.; Konstantinov, A.I.; Zherebker, A.; Lebedev, V.A.; Dubinenkov, I.V.; Kulikova, N.A.; Nikolaev, E.N.; Bulygina, E.; Holmes, R.M. The Structural Arrangement and Relative Abundance of Aliphatic Units May Effect Long-Wave Absorbance of Natural Organic Matter as Revealed by ^{1}H NMR Spectroscopy. *Environ. Sci. Technol.* **2018**, *52*, 12526–12537. [CrossRef]
88. Kholodov, V.A.; Konstantinov, A.I.; Kudryavtsev, A.V.; Perminova, I.V. Structure of humic acids in zonal soils from ^{13}C NMR data. *Eurasian Soil Sci.* **2011**, *44*, 976–983. [CrossRef]

89. Mikhaylova, Y.; Adam, G.; Häussler, L.; Eichhorn, K.J.; Voit, B. Temperature-dependent FTIR spectroscopic and thermoanalytic studies of hydrogen bonding of hydroxyl (phenolic group) terminated hyperbranched aromatic polyesters. *J. Mol. Struct.* **2006**, *788*, 80–88. [CrossRef]
90. Day, K.L. Temperature Dependence of Mid-Infrared Silicate Absorption. *Astrophys. J.* **1976**, *203*, L99. [CrossRef]

Disclaimer/Publisher's Note: The statements, opinions and data contained in all publications are solely those of the individual author(s) and contributor(s) and not of MDPI and/or the editor(s). MDPI and/or the editor(s) disclaim responsibility for any injury to people or property resulting from any ideas, methods, instructions or products referred to in the content.